# An Ultrastable 155-nuclei Silver Nanocluster Protected by Thiacalix[4] arene and Cyclohexanethiol

Zhi Wang,<sup>†</sup> Fahri Alkan,<sup>‡</sup> Christine M. Aikens,<sup>‡</sup> Zhi-Yong Gao,<sup>§</sup> Lei Feng,<sup>†</sup> Mohamedally Kurmoo,<sup>#</sup> Ke-Peng Song,<sup>†</sup> Chen-Ho Tung,<sup>†</sup> Di Sun<sup>\*,†</sup> and Lan-Sun Zheng<sup>&</sup>

†School of Chemistry and Chemical Engineering, State Key Laboratory of Crystal Materials, Shandong University, Ji'nan, 250100, People's Republic of China.

**ABSTRACT:** Thiacalix[4]arenes have emerged as a family of macrocyclic ligands to protect metal nanoparticles, but it remains a great challenge to solve the mystery of their structures at the atomic level, especially for those larger than 2 nm. Here, we report the largest known mixed-valence silver nanocluster [Ag<sub>155</sub>(CyS)<sub>40</sub>(TC4A)<sub>5</sub>Cl<sub>2</sub>] (**Ag155**) protected by deprotonated cyclohexanethiol (CySH) and macrocyclic ligand *p*-tert-butylthiacalix[4]arene (H<sub>4</sub>TC4A). Its single crystal structure consists of a metallic core of four concentric shells, Ag<sub>13</sub>@Ag<sub>42</sub>@Ag<sub>30</sub>@Ag<sub>70</sub>, lined with a protective organic skin of 40 CyS<sup>-</sup> and 5 TC4A<sup>4-</sup> and 2 Cl<sup>-</sup>. **Ag155** manifests an unusual pseudo-5-fold symmetry dictated by the intrinsic metal atom packing and the regioselective distribution of mixed protective ligands. This work not only reveals a macrocyclic ligand effect on the formation of a large silver nanocluster but also provides a new structural archetype for comprehensively perceiving their interface and metal kernel structures.

# INTRODUCTION

Silver nanoclusters have gained increasing attention in terms of their aesthetic structures alongside their promising applications in catalysis, biomedicine, chemical sensing, and biolabeling.1 The atomically-precise elucidation of silver nanocluster structures in the transition size around 2 nm is the overarching goal to understand the quantum size effect and structure-property correlations.<sup>2</sup> Nonetheless, the synthesis and crystallization of silver nanoclusters remain laborious trial-and-error processes so that structures of clusters around 2 nm in size have rarely been reported.3 To date, only a few atomically-precise structures of ~2 nm silver nanoclusters are known including Ag<sub>100</sub>, Ag<sub>136</sub>, Ag<sub>141</sub>, Ag<sub>146</sub>, Ag<sub>180</sub>, Ag<sub>206</sub>, Ag<sub>210-211</sub>, and Ag<sub>374</sub>, which are mostly protected by thiol ligands because of the ease of formation of the robust Ag-S bond.4 In an effort to surmount the synthetic obstacle, a myriad of ligands, e.g. thiol, alkyne, phosphine, amido and their combinations, have been used for the protective monolayer; furthermore, some universal synthetic strategies, e.g. seed growth, anion template, amine-assisted NaBH<sub>4</sub> reduction have been employed to allow silver nanocluster chemistry to blossom.<sup>5</sup> These ligands with some rigidity form diverse interface motifs to protect the silver nanoclusters and also contribute largely to the growth of their single crystals for subsequent crystallographic characterizations. Beyond these conventional ligands, macrocyclic ligands are promising candidates for the construction of polynuclear metal compounds by virtue of their preinstalled multidentate coordination sites;6 however, they markedly lag behind in protecting coinage metal nanoclusters.

Based on the synergistic multidentate chelating effect, one famous family of macrocyclic ligands, thiacalix[4]arenes

(TC4A<sup>4-</sup>), composed of phenolic hydroxyl and bridging sulfur groups in proximity of each other, have been employed to construct polyhedral coordination cages. Awareness of the potential of some macrocyclic organics acting as passivation ligands for metal nanoclusters has been raised only very recently, such as the attempts to install phosphine-calixarene and tetrathiolate-calixarene on gold nanoclusters. Unfortunately, due to their difficult crystallizing nature hampering single crystal X-ray diffraction (SCXRD), their compositions and structures have to be consequently deduced from electrospray ionization mass spectrometry (ESI-MS) and nuclear magnetic resonance spectroscopy (NMR) combined with density functional theory (DFT) calculations.

In spite of the difficulty in crystallization of metal clusters protected by only TC4A<sup>4</sup>, the combination of this bulky one with some small auxiliary ligands may open the door to highquality crystalline products of silver nanoclusters, which, in turn, helps us to understand in detail their molecular and electronic structures.9 In this scenario, some efforts have been devoted to explore the assembly and crystallization conditions of macrocycle ligand-protected silver nanoclusters in the presence of small thiolate or alkyne ligands. The use of macrocyclic ligands to protect metal nanoclusters has been slowly evolving from academic curiosity with poorly identified species to become a synthetic reality by the pioneering work of Wang et al. who reported the first structurally determined TC4A<sup>4-</sup> protected Ag<sub>35</sub> nanocluster. 10 The monolayer of ligands consists of TC4A<sup>4-</sup> and 'BuC≡C<sup>-</sup> distributed to two concentrated regions of the Ag<sub>35</sub> cluster. Very recently, we have presented the synthesis and structural characterization of a C<sub>4</sub>-symmetric Ag<sub>88</sub> "super calix" constructed from eight Ag11 secondary building units encircling a CrO<sub>4</sub><sup>2</sup>- template at the core. 11 That is the highest-nu-

<sup>&</sup>lt;sup>‡</sup>Department of Chemistry, Kansas State University, Manhattan, Kansas 66506, USA.

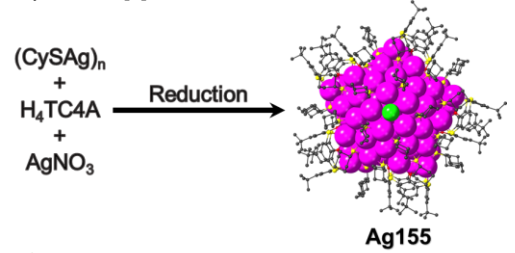
<sup>§</sup>School of Chemistry and Chemical Engineering, Henan Normal University, Xinxiang 453007, People's Republic of China.

<sup>\*</sup>Institut de Chimie de Strasbourg, Université de Strasbourg, CNRS-UMR 7177, 4 rue Blaise Pascal, 67008 Strasbourg Cedex, France.

<sup>&</sup>amp;State Key Laboratory for Physical Chemistry of Solid Surfaces and Department of Chemistry, College of Chemistry and Chemical Engineering, Xiamen University, Xiamen, 361005, P. R. China.

clearity metal cluster based on TC4A<sup>4-</sup> ever reported. Furthermore, we also noted the importance of auxiliary small ligands in this structure that can fill the space between the bulky TC4A<sup>4-</sup> through the naked silver atoms at the surface. They also play an important role to stabilize the overall electronics and geometry of the metal nanoclusters. From these sporadic reports, we found that large-sized silver nanoclusters (> 100 metal atoms) protected by the TC4A<sup>4-</sup> ligand are not yet available. Thus, more efforts are urgently needed to unravel certain chemical fundamentals (*e.g.* metal atom packing, metal-ligand interfacial motif, ligand distribution on the surfaces and so on) of metal nanoclusters protected by such macrocyclic ligand.

**Scheme 1.** Synthesis Route for **Ag155**. CySH = cyclohexanethiol,  $H_4TC4A = p$ -tert-butylthiacalix[4]arene.



- $\sqrt{\text{First silver-TC4A}}$  nanocluster close to 2 nm
- √Pseudo 5-fold symmetry
- √*Ultrastable*

Given the above considerations, herein, a 155-nuclei silver nanocluster  $[Ag_{155}(CyS)_{40}(TC4A)_5Cl_2]$  (Ag155) was successfully synthesized and fully characterized by X-ray crystallography, UV-Vis spectroscopy and ESI-MS. This peculiar nanocluster i) is the first structurally determined silver-TC4A nanocluster with a core size close to 2 nm; ii) has a novel structure consisting of four concentric shells forming an onion-like  $Ag_{13}@Ag_{42}@Ag_{30}@Ag_{70}$  kernel; iii) displays pseudo 5-fold symmetry with mixed TC4A $^4$  and CyS $^-$  ligands showing regioselective coverage on the surface of metal core. This work delivers important insight about the novel metal-TC4A interface and multi-shell metal core structure.

# RESULTS AND DISCUSSION

# **Synthesis Discussion**

The synthesis of Ag155 involving the one-pot reduction of (CySAg)<sub>n</sub> and AgNO<sub>3</sub> in the presence of H<sub>4</sub>TC4A and Et<sub>3</sub>N by NaBH<sub>4</sub> at room temperature is described in Scheme 1 (see details in Supporting Information). Briefly, (CySAg)<sub>n</sub> and AgNO<sub>3</sub> were mixed together in "BuOH followed by a CHCl<sub>3</sub> solution of H<sub>4</sub>TC4A. Subsequently, a freshly prepared ethanolic solution of NaBH4 was added dropwise under vigorous stirring and followed by the addition of Et<sub>3</sub>N. The resulting white turbid solution gradually turned to brown and then black. Finally, the reaction mixture was aged for 6 h in the dark. The solution was filtered, and single crystals of Ag155 suitable for X-ray diffraction were obtained by slow evaporation of the filtrate for three months. Of note, neither other laboratory-available silver salts nor alcohols other than "BuOH work in this system. Other weaker reducing agents such as Ph2SiH2 and NaBH3CN were also tried in this system but Ag155 cannot be isolated. Nevertheless, the reproducibility of Ag155 is very well at the same experiment conditions.

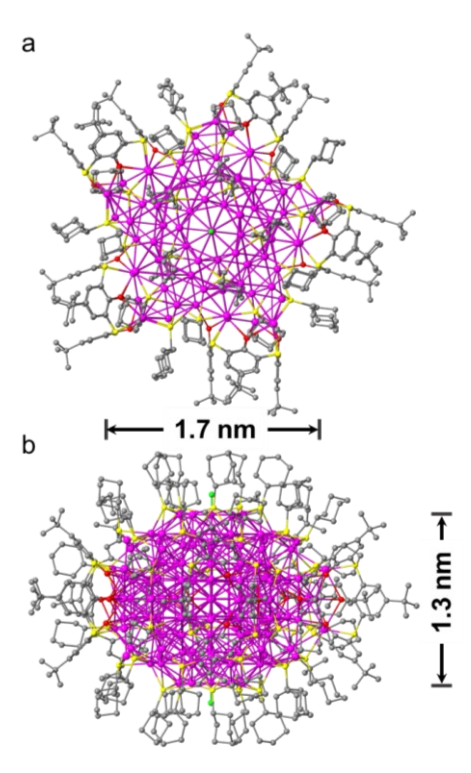


**Figure 1.** Structure of **Ag155**: Top (a) and side (b) views. The molecular dimensions were measured without considering the ligand shell. Color labels: Purple, Ag; yellow, S; green, Cl; gray, C; red, O.

#### X-Ray Structure of Ag155

SCXRD analyses revealed that **Ag155** crystallized in the triclinic space group  $P\ \bar{1}$  (No. 2) with a composition of  $[Ag_{155}(CyS)_{40}(TC4A)_5Cl_2]$ . Based on the X-ray crystallography, we did not directly identify any counter-anions due to their highly disordered orientations in the lattice, but the vibrational bands in infrared ( $v_3 = 1306 \text{ cm}^{-1}$ ) and Raman ( $v_1 = 1005 \text{ cm}^{-1}$ ) spectra clearly proved the counter-anion to be  $NO_3^-$  (Figure S1). Two complete molecules related by the inversion center are packed together per unit cell. An asymmetric unit consists of a complete cluster with a kernel of 155 independent Ag atoms wrapped by 5 TC4A<sup>+</sup>, 40 CyS<sup>-</sup> and 2 Cl<sup>-</sup> (Figure 1). The axial thickness and equatorial diameter of the **Ag155** kernel are 1.3 and 1.7 nm, respectively. The overall morphology of **Ag155** looks like a titoni and the entire **Ag155** exhibits pseudo- $C_{5h}$  symmetry.

For a more detailed dissection of the kernel structure, as illustrated in Figure 2, the arrangement of the 155 silver atoms resembles an onion that can be peeled as four shells  $Ag_{13}@Ag_{42}@Ag_{30}@Ag_{70}$  from inner to outer. All four shells share the same  $C_5$  axis passing through two Cl atoms at two poles. In the innermost shell of the cluster is a 13-silver-atom Ino decahedron (1st shell, Figure 2a and 2e), which is built from two  $Ag_7$  pentagonal bipyramids in an eclipsed conformation through sharing vertices. The  $Ag\cdots Ag$  distances in  $Ag_{13}$  fall in a range of 2.80-2.88 Å (Table S1), which is in agreement with the distances in related silver nanoclusters and almost the same to those in silver metal. This  $Ag_{13}$  shell is caged by an  $Ag_{42}$  shell ( $2^{nd}$  shell), producing a double-shell  $Ag_{55}$  Ino decahedron. The  $Ag_{42}$  shell is an intermediate between the 5-fold symmetric

Ag<sub>32</sub> shell in Ag<sub>206</sub><sup>4f</sup> and the Ag<sub>52</sub> shell in Ag<sub>210</sub>, <sup>4g</sup> which is mandated by the heights of their 1st shell (Figure S2). The Ag...Ag distances in 2<sup>nd</sup> shell are in the range 2.81-3.05 Å (Table S2). This kind of M<sub>55</sub> Ino decahedron with ten (111) facets at two poles and five (100) facets at the equator is an isomer of the  $M_{55}$ Mackay icosahedron observed in Ag<sub>112</sub> and Au<sub>133</sub> (Figure S3). <sup>1</sup> The 3<sup>rd</sup> Ag<sub>30</sub> shell is an opened pentagonal prism (Figure 2c and 2g), which is made up of two face-to-face Ag<sub>15</sub> pentagons. This  $Ag_{30}$  shell is a reduced version of the pentagonal prism in  $Ag_{210}$ (Figure S4) and the average Ag···Ag distance is 2.95 Å (Table S3).  $^{4g}$  The three-shelled Ag<sub>85</sub> is enclosed by the outer Ag<sub>70</sub> semiclosed shell that is formed by two Ag<sub>25</sub> cupolas (pink in Figure 2d, 2h) at the polar sites connecting to five Ag<sub>4</sub> folded rhombuses (purple in Figure 2d, 2h) evenly distributed at the equatorial belt (25×2+4×5=70). This Ag<sub>25</sub> cupola consists of one pentagon, five tetragons and fifteen trigons (Figure S5). Alternatively, it can be seen as ten silver atoms appending on the periphery of a half of a pentagonal cupola ( $J_5$ , one of Johnson solids) by sharing the alternate edges of silver trigons and tetragons. 15 There is a  $C_5$  axis passing through two Cl atoms at the top/bottom poles and a horizontal symmetry-plane at the equator of Ag155 (Figure S6). Due to the absence of a  $C_2$  axis perpendicular to the  $C_5$  axis, the whole symmetry point group is  $C_{5h}$  rather than common  $D_{5h}$ . The average Ag···Ag distances between the 1st and 2nd, 2nd and 3rd, 3rd and 4th shells are 2.89, 2.85, and 2.97 Å, respectively (Table S4, Figure S7).

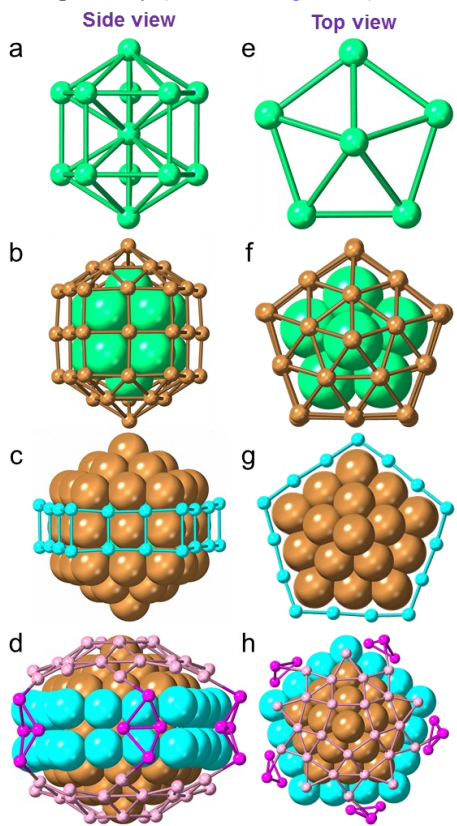


**Figure 2.** Side and top views of the structure dissection of **Ag155** kernel. (a, e) The 1<sup>st</sup> Ag<sub>13</sub> shell (green); (b, f) The 2<sup>nd</sup> Ag<sub>42</sub> shell (brown); (c, g) The 3<sup>rd</sup> Ag<sub>30</sub> shell (cyan); (d, h) The 4<sup>th</sup> Ag<sub>70</sub> shell (pink and purple).

The kernel of the silver nanoparticle is further shielded by a mixture of ligands comprised of 5 TC4A<sup>4-</sup>, 40 CyS<sup>-</sup> and 2 Cl<sup>-</sup>. Five TC4A<sup>4-</sup> can be classified into the three types on the basis of their coordination modes: two of  $\mu_7$ -

 $\kappa_0^4: \kappa_0^3: \kappa_0^3: \kappa_0^3: \kappa_s^1: \kappa_s^1: \kappa_s^1: \kappa_s^1$ two  $\kappa_o^4: \kappa_o^3: \kappa_o^3: \kappa_o^2: \kappa_s^1: \kappa_s^1: \kappa_s^1: \kappa_s^1$ and one of  $\mu_6$ - $\kappa_0^3:\kappa_0^3:\kappa_0^3:\kappa_0^3:\kappa_s^3:\kappa_s^1:\kappa_s^1:\kappa_s^1:\kappa_s^1$  (Figure 3a). Each TC4A<sup>4</sup> not only bound to the Ag<sub>4</sub> folded rhombus on the equatorial belt but also ride on the vertical edge of Ag<sub>30</sub> pentagonal prism (Figure 3b, c). Their bridging sulfur and phenolic oxygen atoms coordinate to Ag to consolidate the outmost and sub-outmost silver shells with Ag-S and Ag-O bond lengths falling within the ranges of 2.53-2.71 and 2.2-2.8 Å, respectively. Different from previously reported Ag<sub>34</sub>, <sup>16</sup> Ag<sub>35</sub> <sup>10</sup> and Ag<sub>88</sub>, <sup>11</sup> the silver atom sitting in the center of the TC4A<sup>4</sup> in Ag155 is coordinated by only three phenolic oxygen atoms, forming seven bonds with silver atoms. The one remaining phenolic oxygen atom is far away from the other three and bound to three or four silver atoms (cyan ball in Figure 3a) in the Ag<sub>30</sub> shell. Owing to the asymmetrical distributions of silver atoms in the lower rim of TC4A<sup>4</sup>, each of them exhibits a distorted configuration with the dihedral angles in the range of 77-136° between the phenyl rings and the plane defined by four oxygen atoms.

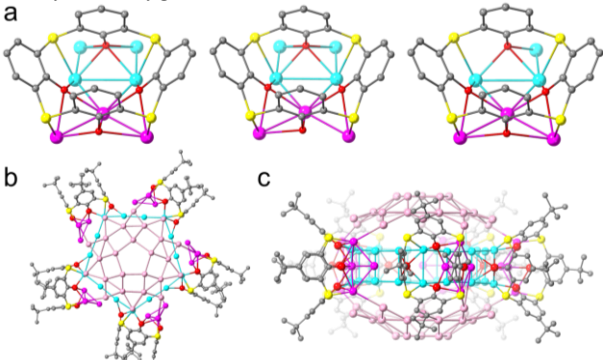


**Figure 3.** (a) The surface motifs formed between TC4A<sup>4</sup> and silver atoms. The tert-butyl groups were removed for clarity. Top (b) and side (c) views of the TC4A<sup>4</sup> ligands bridging the outermost and sub-outermost silver shells. Color labels: Purple, pink and cyan, Ag; yellow, S; gray, C; red, O.

Apart from the five TC4A<sup>4</sup>, there are 40 CyS<sup>-</sup> on the surface. Among them, thirty are bisected to cap on two Ag<sub>25</sub> cupolas up and down, whereas the remaining ten are inserted into the interstices between two adjacent TC4A4- on the equatorial belt. The CyS<sup>-</sup> exhibit two types of bonding motifs, 16  $\mu_3$  and 24  $\mu_4$ , towards silver atoms with the Ag-S bond lengths ranging from 2.39 to 2.96 Å (Figure 4a). As portrayed in Figure 4b and c, the CyS- on the equatorial belt not only ligate to the Ag<sub>4</sub> folded rhombus but also interact with partial silver atoms of the Ag<sub>30</sub> shell. Because of the regioselective distribution of TC4A<sup>4-</sup> and CyS- at the equatorial belt, the shape of the Ag155 resembles a titoni. To complement the coordination vacancy on the silver kernel, two Cl- ions are found to stand on the vertices of the Ag<sub>42</sub> shell with an average Ag-Cl bond distance of 2.64 Å. Upon scrutinization of the synthesis raw material, the Cl<sup>-</sup> is likely formed by the cleavage of the C-Cl bond of CHCl<sub>3</sub>. <sup>17</sup> To the best of our knowledge, Ag155 is the largest silver nanocluster protected by TC4A4-.

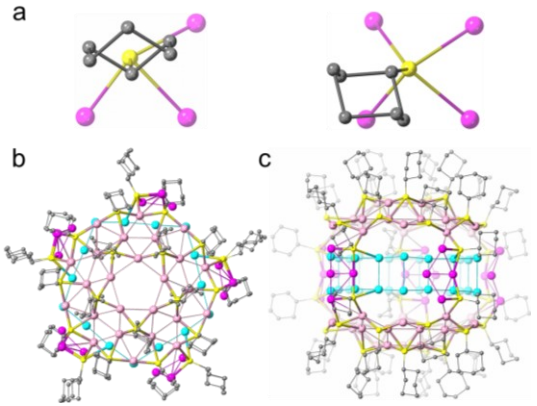


**Figure 4.** (a) The surface motifs formed between CyS<sup>-</sup> and silver atoms. Top (b) and side (c) views of the CyS<sup>-</sup> ligands bridging the outermost and sub-outermost silver shells. Color labels: Purple, pink and cyan, Ag; yellow, S; gray, C.

# ESI-MS and TEM of Ag155

ESI-MS has been implemented as an effective method to verify the composition and assembly mechanism of metal nanoclusters in the realm of cluster chemistry. 18 Therefore, the ESI-MS of Ag155 dissolved in CHCl<sub>3</sub> was performed in both positive and negative ion modes. No informative signal was detected in the negative-ion mode, but one envelop centered at m/z12492.242 (1a) was observed in positive ion mode with the pre plus storage time of 90 µs (Figure 5a). Its charge state, determined by the separation of isotope peaks, is +2. After careful comparison of experimental and simulated isotopic envelops, composition exactly assigned  $[Ag_{155}(CyS)_{40}(TC4A)_5Cl_2]^{2+}$ (Calcd. 12492.296), which matches well with the formula determined by X-ray crystallography.

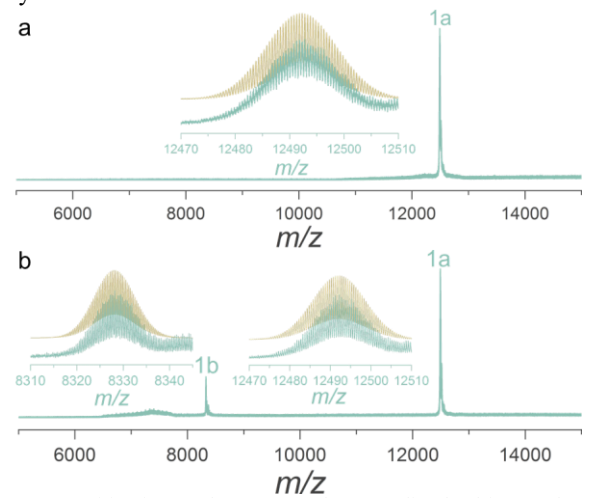


**Figure 5.** Positive-ion mode ESI-MS of **Ag155** dissolved in CHCl<sub>3</sub> with different pre plus storage time parameters: (a) 90  $\mu$ s and (b) 70  $\mu$ s. Insets: The experimental (blue lines) and simulated (yellow lines) isotope-distribution patterns of **1a** and **1b**.

What is more fascinating is that an envelope was additionally detected at m/z 8328.165 (**1b**) when the pre plus storage time parameter was shortened from 90 to 70  $\mu$ s (Figure 5b). The other peak belongs to a +3 species which perfectly agrees with  $[Ag_{155}(CyS)_{40}(TC4A)_5Cl_2]^{3+}$  (Calcd. 8328.197). Generally

speaking, the pre plus storage is a decay for collecting ions between the transfer time and time of flight pulser on. The shorter pre plus storage time facilitates the transfer of lighter ions to the detector, which is consistent with the phenomenon we observed above.

The high-angle annular dark-field scanning transmission electron microscopy (HAADF-STEM) images taken in three different regions show a high degree of homogeneity of the nanoparticles in both size and shape. The measured average diameters of nanoparticles are 1.324±0.083, 1.337±0.110 and 1.308±0.041 nm, respectively, consistent with the pole-to-pole distance (1.3 nm) of Ag155 determined by SCXRD (Figure S8). Nonspherical Ag155, capped by the anisotropic arrangement of surface ligands, TC4A<sup>4-</sup> and CyS<sup>-</sup>, shows such a homogeneous size under the TEM, which suggests that they may align on carbon substrate with a unified orientation, dictated by interfacial energy mainly involving hydrophobic interactions at the interface between the carbon substrate and nanocluster. Combing with above ESI-MS results, we can conclude that Ag155 is highly stable in CHCl<sub>3</sub> solution, even under the ESI-MS condition.

# **Optical Properties and DFT Calculations**

The UV-Vis-NIR spectrum of Ag155 was acquired in the wavelength range 300-900 nm (Figure 6). A pronounced peak was observed at 460 nm, consistent with the surface plasmon bands of the silver nanoclusters of size reaching close to 2 nm. 4b. 4c, 4d, 4g The CHCl<sub>3</sub> solution of Ag155 is stable for at least 36 hours at room temperature (Figure S9). Based on ESI-MS results, we found the dominant species to be positively-charged, such as [Ag<sub>155</sub>(CyS)<sub>40</sub>(TC4A)<sub>5</sub>Cl<sub>2</sub>]<sup>2+</sup>. In solution, the formula may be [Ag<sub>155</sub>(CyS)<sub>40</sub>(TC4A)<sub>5</sub>Cl<sub>2</sub>]<sup>1+</sup>, with a single NO<sub>3</sub><sup>-</sup> counterion. The dication would possess 91 free valence electrons whereas the monocation possesses 92 free valence electrons (92 = 155 (Ag) - 20 (TC4A) - 40 (CyS) - 2(Cl) - 1(z)) with a delosuperatomic orbital filling calized written  $1S^{2}|1P^{6}|1D^{10}|2S^{2}1F^{14}|2P^{6}1G^{18}|2D^{10}3S^{2}1H^{22}|.$ This shell-closing electron count falls in the "magic" number series (2, 8, 18, 34, 58, 92),<sup>20</sup> so **Ag155** is expected to be an electron shell closing system.

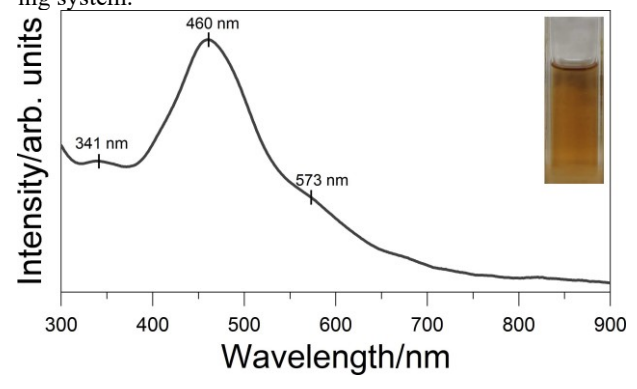


Figure 6. The ultraviolet–visible absorption spectrum of Ag155 recorded in CHCl<sub>3</sub> at room temperature. Inset: photograph of Ag155 solution.

To further understand the electronic structure of Ag155, we performed density functional theory (DFT) calculations. In Figure 7a, we show the partial and total density of states (DOS)

curves for the model  $[Ag_{155}(SH)_{40}(TC4A)_5Cl_2]^{1+}$  cluster (abbreviated as  $Ag_{155}$  in this section, Figure S10). The HOMO-LUMO gap is calculated to be 0.41 eV. Partial DOS curves show that atomic Ag s and p orbitals largely contribute to the low-lying occupied and unoccupied levels of the cluster. The p orbitals of S, O and C also contribute to the low-lying occupied levels considerably, whereas their contribution to the unoccupied levels is somewhat smaller. Total DOS curve exhibits an intense feature for the -8 to -12 eV energy range of the electronic structure, which mainly originates from the Ag d band as seen from the partial DOS curves and energy levels.

In Figure 7b, we show the calculated UV-Vis spectrum for the Ag<sub>155</sub> cluster, along with the stick spectrum that only shows

transitions with oscillator strengths larger than 0.02. Overall, the calculated spectrum shows a good agreement with the experimental spectrum shown in Figure 6. The main feature in the theoretical spectrum is an intense peak around 2.9 eV. As shown in the stick spectrum, this feature originates from several closely-spaced transitions. It should be noted that the energy and the origin of this peak is quite similar to the plasmonic peak from the recently investigated  $Ag_{211}$  cluster. In addition to the intense feature at 2.9 eV, the spectrum of the  $Ag_{155}$  cluster also exhibits a shoulder around 2.5 eV and a broad peak centered around 2.0 eV. Unlike the peak at 2.9 eV, these features mainly originate from a small number of scattered transitions.

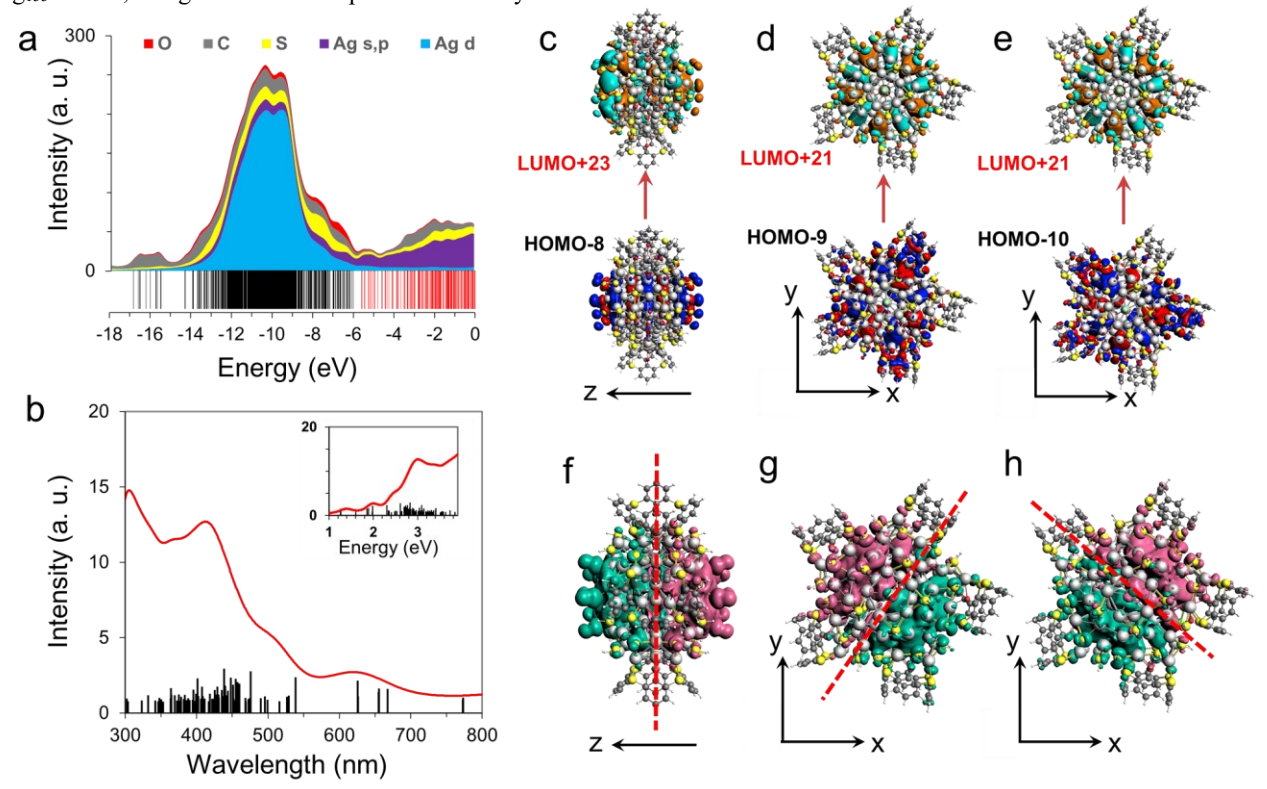


Figure 7. (a) Partial and total DOS curves of the Ag<sub>155</sub> cluster. (b) Calculated UV-vis spectrum (red) and the stick spectrum of excited states with oscillator strengths larger than 0.02 a.u. (black). (c) Illustration of occupied and unoccupied molecular orbitals for HOMO-8 $\rightarrow$ LUMO+23 transition. (d) Occupied and unoccupied molecular orbitals for HOMO-10 $\rightarrow$ LUMO+21 transition. (e) Occupied and unoccupied molecular orbitals for HOMO-10 $\rightarrow$ LUMO+21 transition. (f) TFD of the excited state resulting from the constructive coupling of configurations with transition-dipole moment along the  $C_5$  axis. (g) and (h) TFD of the excited state resulting from the constructive coupling of configurations with transition-dipole moment orthogonal to the unique  $C_5$  axis.

In Figure 7c-e, we show the occupied $\rightarrow$ unoccupied pairs with the largest oscillator strengths for the Ag<sub>155</sub> cluster. As seen from the figure, these orbitals mainly originate from the Ag s and p band of the electronic structure. The HOMO-8 $\rightarrow$ LUMO+23 transition (Figure 7c) exhibits the largest oscillator strength among the possible transitions. The nodes of both orbitals lie on the unique  $C_5$  axis (z) of the cluster, which results in a transition-dipole moment along this axis. In comparison, transition-dipole moments (x, y) of HOMO-9 $\rightarrow$ LUMO+21 (Figure 7d) and HOMO-10 $\rightarrow$ LUMO+21 (Figure 7e) transitions are orthogonal to the  $C_5$  axis of the cluster.

To further understand the origin of spectral features, we perform a restricted TDDFT+TB excited-state calculation where only the occupied  $\rightarrow$  unoccupied pairs with oscillator strengths larger than 0.5 are included in the configuration interaction (CI).

As a result of this restriction, the CI space is reduced to only 16 configurations, which greatly simplifies our analysis. Detailed excited state information of selective states is given in Table S7. From the results of this analysis, it is seen that constructive coupling of high-oscillator-strength configurations, which exhibit a transition-dipole moment along the  $C_5$  axis, result in an excited state at 2.80 eV. The transition-fit density (TFD) of this excited state shows a large dipole along the  $C_5$  axis as shown in Figure 7f. In comparison, constructive coupling of configurations with a transition-dipole moment orthogonal to the  $C_5$  axis results in two approximately degenerate excited states at 1.95 eV. Similarly, TFDs exhibit a large dipole orthogonal to the  $C_5$  axis as shown in Figure 7g and 7h. We note that the energies of these excited states agree well with the energies of spectral features shown in Figure 7b. These results show that the constructive

coupling of these configurations with transition-dipole moments along the  $C_5$  axis primarily contribute to the intense peak at ~2.9 eV (Figure 7b), whereas configurations with transition-dipole moments orthogonal to the  $C_5$  axis mostly contribute to the peak at ~2.0 eV.

## Photothermal performance

Based on such atom-precise structure, we further explored if it can induce an intense photothermal effect. First of all, Ag155 was dispersed in chloroform with different concentrations ranging from 60 to 240 µM, and then irradiated with a 660 nm laser at the low power density of 100 mW cm<sup>-2</sup>. As shown in Figure 8a, the temperatures of them all increase under the laser irradiation, indicating Ag155 possess the ability of photothermal conversion. The temperatures are proportional to the Ag155 concentrations, which are all reached their plateaus at 41.4, 53.9 and 59.1 °C within 300 s, respectively (Figure 8b). The maximum temperatures are almost constant without significant attenuation in 6 cycles heating and cooling processes (Figure 8c). Furthermore, the comparable UV-Vis spectra of Ag155 before and after irradiation verified the excellent photothermal stability of the nanocluster (Figure S11). No obvious temperature fluctuation (t < 1 °C) was detected in blank chloroform, corroborating that the temperature variations under the laser irradiation are all contributed by Ag155. An dramatically temperature increase from 20 to 59.1 °C is observed within 300 s irradiation, which is found to be much better than those of some common materials reported in the literature, such as azobenzene derivatives and nanobioconjugates.<sup>21</sup> This is mainly because no fluorescence is observed in Ag155 under the irradiation of 660 nm, suggesting very weak radiative migration. Therefore, photothermal conversion become the overriding method of energy release.

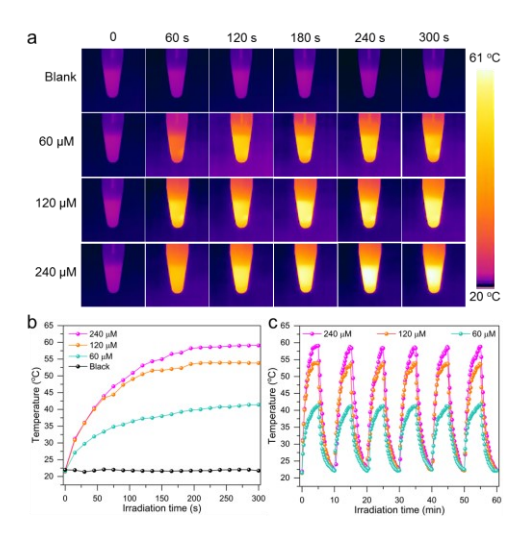


**Figure 8.** (a) IR images recorded with a thermal imaging camera at different irradiation times. (b) Plots of temperature rise of different concentrations of **Ag155** solution and blank solvent with time. (c) Photothermal heating and natural cooling cycles under 660 nm laser irradiation with power density of 100 mW cm<sup>-2</sup>.

# CONCLUSIONS

To summarize, an unprecedented 155-nuclei silver nanocluster was synthesized and its structure was determined by X-ray crystallography. It is a multishell structure consisting of a concentric Ag<sub>13</sub>@Ag<sub>42</sub>@Ag<sub>30</sub>@Ag<sub>70</sub> kernel protected by 5 TC4A<sup>4-</sup>, 40 CyS<sup>-</sup> and 2 Cl<sup>-</sup>. As the largest silver nanocluster based on the macrocyclic thiacalix[4]arene ligand, **Ag155** exhibits pseudo 5-fold symmetry due to the regioselective coordination of TC4A<sup>4-</sup> and CyS<sup>-</sup> on the surface of the silver nanocluster as well as the intrinsic metal atom packing. The successful incorporation of TC4A<sup>4-</sup> on this silver nanocluster paves a brand new avenue for the synthesis of large-sized silver nanoclusters and provides direct evidence to decipher the electronic and interface structures of silver nanoparticles.

#### ASSOCIATED CONTENT

**Supporting Information**. Experimental and computational details, detailed crystallographic structure and data including the CIF file, PXRD, EDX mapping, UV-Vis, HAADF-STEM, Raman and IR. This information is available free of charge via the internet at http://pubs.acs.org.

#### **AUTHOR INFORMATION**

#### **Corresponding Author**

dsun@sdu.edu.cn (D. S.)

#### **ORCID**

Di Sun: 0000-0001-5966-1207

Christine Aikens: 0000-0002-0854-7997

Zhi Wang: 0000-0001-8315-3501

# Notes

The authors declare no competing financial interest.

# **ACKNOWLEDGMENT**

This work was financially supported by the National Natural Science Foundation of China (Grant Nos. 22171164, 91961105, 21822107, 21827801), the Natural Science Foundation of Shandong Province (Nos. ZR2020ZD35 and ZR2019ZD45), the Fok Ying Tong Education Foundation (171009), the Taishan Scholar Project of Shandong Province of China (Nos. tsqn201812003 and ts20190908), the Qilu Youth Scholar Funding of Shandong University, the National Postdoctoral Innovative Talents Support Program (No. BX2021171), China Postdoctoral Science Foundation (No. 2021M700081), Project for Scientific Research Innovation Team of Young Scholar in Colleges and Universities of Shandong Province (2019KJC028). C.M.A was supported by the National Science Foundation (CHE-1905048) of the United States. The computing for this project was performed on the Beocat Research Cluster at Kansas State University, which is funded in part by NSF grants CHE-1726332, CNS-1006860, EPS-1006860, and EPS-0919443. We thank Mohamedally Kurmoo of Université de Strasbourg for useful discussions.

# REFERENCES

- (a) Yan, J.; Teo, B. K.; Zheng, N., Surface chemistry of atomically precise coinage-metal nanoclusters: from structural control to surface reactivity and catalysis. Acc. Chem. Res. 2018, 51 (12), 3084-3093. (b) Du, X.; Jin, R., Atomically precise metal nanoclusters for catalysis. Acs Nano 2019, 13 (7), 7383-7387. (c) Sharma, S.; Chakrahari, K. K.; Saillard, J.-Y.; Liu, C. W., Structurally precise dichalcogenolate-protected copper and silver superatomic nanoclusters and their alloys. Acc. Chem. Res. 2018, 51 (10), 2475-2483. (d) Yu, H.; Rao, B.; Jiang, W.; Yang, S.; Zhu, M., The photoluminescent metal nanoclusters with atomic precision. Coord. Chem. Rev. 2019, 378, 595-617. (e) Schnepf, A.; Schnockel, H., Nanoscale molecular silver cluster compounds in gram quantities. Angew Chem Int Ed 2014, 53 (12), 3064-3066. (f) Wilson, R. J.; Lichtenberger, N.; Weinert, B.; Dehnen, S., Intermetalloid and heterometallic clusters combining pblock (Semi)metals with d- or f-block metals. Chem. Rev. 2019, 119 (14), 8506-8554. (g) Yao, Q.; Yuan, X.; Chen, T.; Leong, D. T.; Xie, J., Engineering functional metal materials at the atomic level. Adv. Mater. 2018, 30 (47), 1802751.
- (a) Yan, N.; Xia, N.; Liao, L. W.; Zhu, M.; Jin, F. M.; Jin, R. C.; Wu, Z. K., Unraveling the long-pursued Au<sub>144</sub> structure by x-ray crystallography. *Sci Adv* 2018, 4 (10), eaat7259. (b) Wu, Z.; Yao, Q.; Zang, S.; Xie, J., Directed self-assembly of ultrasmall metal nanoclusters. *ACS Materials Lett.*, 2019, 1 (2), 237-248.
- Yonesato, K.; Ito, H.; Itakura, H.; Yokogawa, D.; Kikuchi, T.; Mizuno, N.; Yamaguchi, K.; Suzuki, K., Controlled assembly synthesis of atomically precise ultrastable silver nanoclusters with polyoxometalates. J. Am. Chem. Soc. 2019, 141 (50), 19550-19554.
- 4) (a) Zhu, M.; Ma, X.; Bai, Y.; Song, Y.; Li, Q.; Lv, Y.; Zhang, H.; Yu, H., A rhombicuboctahedral Ag<sub>100</sub>: four-layered octahedral silver nanocluster adopting the russian nesting doll model. Angew. Chem. Int. Ed. 2020, 59 (39), 17234-17238. (b) Yang, H.; Wang, Y.; Chen, X.; Zhao, X.; Gu, L.; Huang, H.; Yan, J.; Xu, C.; Li, G.; Wu, J.; Edwards, A. J.; Dittrich, B.; Tang, Z.; Wang, D.; Lehtovaara, L.; Hakkinen, H.; Zheng, N., Plasmonic twinned silver nanoparticles with molecular precision. Nat Commun 2016, 7, 12809. (c) Ren, L.; Yuan, P.; Su, H.; Malola, S.; Lin, S.; Tang, Z.; Teo, B. K.; Hakkinen, H.; Zheng, L.; Zheng, N., Bulky surface ligands promote surface reactivities of  $[Ag_{141}X_{12}(S-Adm)_{40}]^{3+}$  (X = Cl, Br, I) nanoclusters: models for multiple-twinned nanoparticles. J. Am. Chem. Soc. 2017, 139 (38), 13288-13291. (d) Song, Y.; Lambright, K.; Zhou, M.; Kirschbaum, K.; Xiang, J.; Xia, A.; Zhu, M.; Jin, R., Large-scale synthesis, crystal structure, and optical properties of the Ag<sub>146</sub>Br<sub>2</sub>(SR)<sub>80</sub> nanocluster. ACS Nano 2018, 12 (9), 9318-9325. (e) Wang, Z.; Su, H.-F.; Tan, Y.-Z.; Schein, S.; Lin, S.-C.; Liu, W.; Wang, S.-A.; Wang, W.-G.; Tung, C.-H.; Sun, D.; Zheng, L.-S., Assembly of silver trigons into a buckyball-like Ag<sub>180</sub> nanocage. Proc Natl Acad Sci USA 2017, 114 (46), 12132-12137.(f) Yan, J.; Zhang, J.; Chen, X.; Malola, S.; Zhou, B.; Selenius, E.; Zhang, X.; Yuan, P.; Deng, G.; Liu, K.; Su, H.; Teo, B. K.; Hakkinen, H.; Zheng, L.; Zheng, N., Thiol-stabilized atomically precise, superatomic silver nanoparticles for catalysing cycloisomerization of alkynyl amines. Natl Sci Rev, 2018, 5 (5), 694-702. (g) Liu, J.-Y.; Alkan, F.; Wang, Z.; Zhang, Z.-Y.; Kurmoo, M.; Yan, Z.; Zhao, Q.-Q.; Aikens, C. M.; Tung, C.-H.; Sun, D., Different silver nanoparticles in one crystal: Ag<sub>210</sub>(PrPhS)<sub>71</sub>(Ph<sub>3</sub>P)<sub>5</sub>Cl and Ag<sub>211</sub>(<sup>i</sup>PrPhS)<sub>71</sub>(Ph<sub>3</sub>P)<sub>6</sub>Cl. Angew. Chem. Int. Ed. 2019, 58 (1),
- (a) Lei, Z.; Wan, X.-K.; Yuan, S.-F.; Guan, Z.-J.; Wang, Q.-M., Alkynyl approach toward the protection of metal nanoclusters. *Acc. Chem. Res.* 2018, 51 (10), 2465-2474. (b) AbdulHalim, L. G.; Bootharaju, M. S.; Tang, Q.; Del Gobbo, S.; AbdulHalim, R. G.; Eddaoudi, M.; Jiang, D.-e.; Bakr, O. M., Ag<sub>29</sub>(BDT)<sub>12</sub>(TPP)<sub>4</sub>: a tetravalent nanocluster. *J. Am. Chem. Soc.* 2015, 137 (37), 11970-11975. (c) Joshi, C. P.; Bootharaju, M. S.; Alhilaly, M. J.; Bakr, O. M., [Ag<sub>25</sub>(SR)<sub>18</sub>]: the "golden" silver nanoparticle. *J. Am. Chem. Soc.* 2015, 137 (36), 11578-11581. (d) Ghosh, A.; Bodiuzzaman, M.; Nag, A.; Jash, M.; Baksi, A.; Pradeep, T., Sequential dihydrogen desorption from hydride-protected atomically precise silver clusters and the formation of naked clusters in the gas phase. *ACS Nano* 2017, 11 (11), 11145-11151. (e) Liu, X.; Chen, J.; Yuan, J.; Li, Y.; Li, J.; Zhou, S.; Yao, C.; Liao, L.; Zhuang, S.; Zhao, Y.; Deng, H.; Yang, J.; Wu, Z., A silver nanocluster containing interstitial sulfur and unprecedented

- chemical bonds. *Angew. Chem. Int. Ed.* **2018**, *57* (35), 11273-11277. (f) Yuan, S.-F.; Guan, Z.-J.; Liu, W.-D.; Wang, Q.-M., Solvent-triggered reversible interconversion of all-nitrogen-donor-protected silver nanoclusters and their responsive optical properties. *Nat Commun* **2019**, *10*, 4032. (g) Wang, Z.; Su, H.-F.; Kurmoo, M.; Tung, C.-H.; Sun, D.; Zheng, L.-S., Trapping an octahedral Ag<sub>6</sub> kernel in a seven-fold symmetric Ag<sub>56</sub> nanowheel. *Nat Commun* **2018**, *9*, 2094.
- (a) Fang, Y.; Deng, Y.; Dehaen, W., Tailoring pillararene-based receptors for specific metal ion binding: from recognition to supramolecular assembly. Coord. Chem. Rev. 2020, 415, 213313. (b) Neri, P., Sessler, J. L., Wang, M.-X., Eds.; Calixarenes and beyond. Springer: Cham, Switzerland, 2016. (c) Kumar, R.; Lee, Y. O.; Bhalla, V.; Kumar, M.; Kim, J. S., Recent developments of thiacalixarene based molecular motifs. Chem. Soc. Rev., 2014, 43 (13), 4824-4870. (d) Sliwa, W.; Kozlowski, C. Calixarenes and Resorcinarenes: Synthesis, Properties and Applications; Wiley-VCH: Weinheim, Germany, 2009.
- (a) Liu, M.; Liao, W.; Hu, C.; Du, S.; Zhang, H., Calixarene-based nanoscale coordination cages. *Angew. Chem. Int. Ed.* 2012, 51 (7), 1585-1588. (b) Bi, Y.; Wang, X.-T.; Liao, W.; Wang, X.; Wang, X.; Zhang, H.; Gao, S., A {Co<sub>32</sub>} nanosphere supported by *p*-tert-butylthiacalix[4] arene. *J. Am. Chem. Soc.* 2009, 131 (33), 11650-11651. (c) Hang, X.; Liu, B.; Zhu, X.; Wang, S.; Han, H.; Liao, W.; Liu, Y.; Hu, C., Discrete {Ni<sub>40</sub>} coordination cage: a calixarene-based Johnson-type (J<sub>17</sub>) hexadecahedron. *J. Am. Chem. Soc.* 2016, 138 (9), 2969-2972. (d) Su, K.; Jiang, F.; Qian, J.; Wu, M.; Gai, Y.; Pan, J.; Yuan, D.; Hong, M., Open pentameric calixarene nanocage. *Inorg Chem* 2014, 53 (1), 18-20. (e) Xiong, K.-C.; Jiang, F.-L.; Gai, Y.-L.; Yuan, D.-Q.; Han, D.; Ma, J.; Zhang, S.-Q.; Hong, M.-C., Chlorine-induced assembly of a cationic coordination cage with a μ<sub>5</sub>-carbonato-bridged Mn<sup>II</sup><sub>24</sub> core. *Chem-Eur J* 2012, 18 (18), 5536-5540.
- (a) de Silva, N.; Ha, J.-M.; Solovyov, A.; Nigra, M. M.; Ogino, I.; Yeh, S. W.; Durkin, K. A.; Katz, A., A bioinspired approach for controlling accessibility in calix[4]arene-bound metal cluster catalysts. *Nat Chem* 2010, 2 (12), 1062-1068. (b) Hassinen, J.; Pulkkinen, P.; Kalenius, E.; Pradeep, T.; Tenhu, H.; Hakkinen, H.; Ras, R. H. A., Mixed-monolayer-protected Au<sub>25</sub> clusters with bulky calix[4]arene functionalities. *J. Phys. Chem. Lett.* 2014, 5 (3), 585-589.
- Wang, Z.-Y.; Wang, M.-Q.; Li, Y.-L.; Luo, P.; Jia, T.-T.; Huang, R.-W.; Zang, S.-Q.; Mak, T. C. W., Atomically precise site-specific tailoring and directional assembly of superatomic silver nanoclusters. J. Am. Chem. Soc. 2018, 140 (3), 1069-1076.
- Guan, Z.-J.; Zeng, J.-L.; Nan, Z.-A.; Wan, X.-K.; Lin, Y.-M.; Wang, Q.-M., Thiacalix[4]arene: new protection for metal nanoclusters. Sci. Adv. 2016, 2 (8), e1600323.
- Wang, Z.; Su, H.-F.; Gong, Y.-W.; Qu, Q.-P.; Bi, Y.-F.; Tung, C.-H.; Sun, D.; Zheng, L.-S., A hierarchically assembled 88-nuclei silver-thiacalix[4]arene nanocluster. *Nat Commun* 2020, 11, 308.
- (a) Nakamoto, K. Infrared and Raman spectra of inorganic and coordination compounds; Wiley, 1963. (b) Rajkumar, B. J. M.; Ramakrishnan, V., Infrared and raman spectra of L-valine nitrate and Lleucine nitrate. J. Raman Spectrosc. 2000, 31 (12), 1107-1112.
- (a) Desireddy, A.; Conn, B. E.; Guo, J.; Yoon, B.; Barnett, R. N.; Monahan, B. M.; Kirschbaum, K.; Griffith, W. P.; Whetten, R. L.; Landman, U.; Bigioni, T. P., Ultrastable silver nanoparticles. *Nature* 2013, 501 (7467), 399-402. (b) Yan, J.; Su, H.; Yang, H.; Malola, S.; Lin, S.; Haekkinen, H.; Zheng, N., Total structure and electronic structure analysis of doped thiolated silver [MAg<sub>24</sub>(SR)<sub>18</sub>]<sup>2-</sup> (M = Pd, Pt) clusters. *J. Am. Chem. Soc.* 2015, 137 (37), 11880-11883.
- (a) Hu, F.; Li, J.-J.; Guan, Z.-J.; Yuan, S.-F.; Wang, Q.-M., Formation of an alkynyl-protected Ag<sub>112</sub> silver nanocluster as promoted by chloride released in situ from CH<sub>2</sub>Cl<sub>2</sub>. Angew. Chem. Int. Ed. 2020, 59(13), 5312–5315. (b) Zeng, C.; Chen, Y.; Kirschbaum, K.; Appavoo, K.; Sfeir, M. Y.; Jin, R., Structural patterns at all scales in a nonmetallic chiral Au<sub>133</sub>(SR)<sub>52</sub> nanoparticle. Sci. Adv. 2015, 1 (2), e150004.
- Johnson, J., N. W., Convex polyhedra with regular faces. Canadian Journal of Mathematics 1966, 18 (1), 169-200.

- 16) Guan, Z.-J.; Hu, F.; Yuan, S.-F.; Nan, Z.-A.; Lin, Y.-M.; Wang, Q.-M., The stability enhancement factor beyond eight-electron shell closure in thiacalix[4]arene-protected silver clusters. *Chem Sci* 2019, 10 (11), 3360-3365.
- (a) Ghosh, A.; Huang, R.-W.; Alamer, B.; Abou-Hamad, E.; Hedhili, M. N.; Mohammed, O. F.; Bakr, O. M., [Cu<sub>61</sub>(S'Bu)<sub>26</sub>S<sub>6</sub>Cl<sub>6</sub>H<sub>14</sub>]<sup>+</sup>: a core-shell superatom nanocluster with a quasi-J<sub>36</sub> Cu<sub>19</sub> core and an "18-crown-6" metal-sulfide-like stabilizing belt. ACS Materials Lett.
  2019, 1 (3), 297-302. (b) Bian, S.-D.; Wang, Q.-M., Snowman-like silver alkynyl cluster consolidated by templating chloride and peripheral trifluoroacetates. Chem Commun 2008, (43), 5586-5588.
- (a) Hirata, K.; Tomihara, R.; Kim, K.; Koyasu, K.; Tsukuda, T., Characterization of chemically modified gold and silver clusters in gas phase. Phys. Chem. Chem. Phys., 2019, 21 (32), 17463-17474. (b) Chen, T.; Yao, Q.; Nasaruddin, R. R.; Xie, J., Electrospray ionization mass spectrometry: a powerful platform for noble-metal nanocluster analysis. Angew. Chem. Int. Ed. 2019, 58 (35), 11967-11977. (c) Kang, X.; Wang, S.; Zhu, M., Observation of a new type of aggregation-induced emission in nanoclusters. Chem Sci 2018, 9 (11), 3062-3068. (d) Kang, X.; Wei, X.; Jin, S.; Yuan, Q.; Luan, X.; Pei, Y.; Wang, S.; Zhu, M.; Jin, R., Rational construction of a library of M<sub>29</sub> nanoclusters from monometallic to tetrametallic. Proc Natl Acad Sci USA 2019, 116 (38), 18834-18840. (e) Chakraborty, P.; Baksi, A.; Khatun, E.; Nag, A.; Ghosh, A.; Pradeep, T., Dissociation of gas phase ions of atomically precise silver clusters reflects their solution phase stability. J. Phys. Chem., C 2017, 121 (20), 10971-10981. (f) Schenk, C.; Kracke, A.; Fink, K.; Kubas, A.; Klopper, W.;

- Neumaier, M.; Schnockel, H.; Schnepf, A., The formal combination of three singlet biradicaloid entities to a singlet hexaradicaloid metalloid Ge<sub>14</sub>[Si(SiMe<sub>3</sub>)<sub>3</sub>]<sub>5</sub>[Li(THF)<sub>2</sub>]<sub>3</sub> cluster. *J. Am. Chem. Soc.* **2011**, *133* (8), 2518-2524.
- (a) Mingos, D. M. P.; Lin, Z. Structural consequences of the Jellium model for alkali-metal clusters. *Chem. Phys.* 1989, *137*, 15–24. (b) Teo, B. K.; Yang, S. Y. Jelliumatic shell model. *J. Cluster Sci.* 2015, *26*, 1923–1941. (c) Walter, M.; Akola, J.; Lopez-Acevedo, O.; Jadzinsky, P. D.; Calero, G.; Ackerson, C. J.; Whetten, R. L.; Groenbeck, H.; Hakkinen, H., A unified view of ligand-protected gold clusters as superatom complexes. *Proc Natl Acad Sci USA* 2008, *105* (27), 9157-9162.
- (a) Reveles, J. U.; Khanna, S. N.; Roach, P. J.; Castleman, A. W., Multiple valence superatoms. *Proc Natl Acad Sci USA* **2006**, *103* (49), 18405-18410. (b) Luo, Z. X.; Castleman, A. W., Special and General Superatoms. *Acc. Chem. Res.*, **2014**, *47* (10), 2931-2940.
- 21) (a) Lyu, Y.; Xie, C.; Chechetka, S. A.; Miyako, E.; Pu, K., Semiconducting Polymer Nanobioconjugates for Targeted Photothermal Activation of Neurons. *J Am Chem Soc* 2016, *138* (29), 9049-9052. (b) Mao, F.; Wen, L.; Sun, C.; Zhang, S.; Wang, G.; Zeng, J.; Wang, Y.; Ma, J.; Gao, M.; Li, Z., Ultrasmall Biocompatible Bi<sub>2</sub>Se<sub>3</sub> Nanodots for Multimodal Imaging-Guided Synergistic Radiophotothermal Therapy against Cancer. *Acs Nano* 2016, *10* (12), 11145-11155. (c) Wu, Z.; Ji, C.; Zhao, X.; Han, Y.; Muellen, K.; Pan, K.; Yin, M., Green-Light-Triggered Phase Transition of Azobenzene Derivatives toward Reversible Adhesives. *J Am Chem Soc* 2019, *141* (18), 7385-7390.

# Table of Content

